SCIENTIFIC REPORTS

OPEN

SUBJECT AREAS:
PRE-CLINICAL STUDIES
MEDICAL RESEARCH
LIVER CANCER

Received
10 January 2014

Accepted
19 June 2014

Published
15 August 2014

Correspondence and requests for materials should be addressed to J.S. (xnqiuqiu@163.com) or X.-P.Z. (zxp@bjcancer.org)

Applicable apparent diffusion coefficient of an orthotopic mouse model of gastric cancer by improved clinical MRI diffusion weighted imaging

Jia Sun[1], Xiao-Peng Zhang[2], Xiao-Ting Li[2], Lei Tang[2], Yong Cui[2], Xiao-Yan Zhang[2] & Ying-Shi Sun[2]

[1]Department of Radiology; Beijing Chao-Yang Hospital, 8 Gongren Tiyuchang Nanlu, Chaoyang District, Beijing, 100020, China, [2]Key Laboratory of Carcinogenesis and Translational Research (Ministry of Education), Department of Radiology, Peking University Cancer Hospital & Institute. No.52, Fucheng Road, Haidian District, Beijing, 100142, China.

In vivo **imaging studies in animal models are hindered by variables that contribute to poor image quality and measurement reliability. As such we sought to improve the diffusion coefficient (ADC) of an orthotopic mouse model of gastric cancer in diffusion-weighted images (DWI) using alginate moulding and Ultrasonic coupling medium. BGC-823 human gastric cancer cells were subcutaneously injected into the abdomen of nude mice and 1 mm^3 primary tumour was orthotopically transplanted. Alginate and coupling medium were applied to the mice and MRI (T2 and DWI) was performed for 6 weeks. Regions of interest (ROI) were drawn and liver and tumour ADC were evaluated. Using alginate moulding, the mean quality total score of DW imaging was 8.53; however, in control animals this value was 5.20 ($p < 0.001$). The coefficient of variation of ADC of liver in experimental and control groups were 0.071 and 0.270 ($p < 0.001$), respectively, suggesting this method may be helpful for DWI studies of important human diseases such as gastric cancer.**

Diffusion weighted imaging (DWI) is a widely utilized magnetic resonance imaging (MRI) technique that provides *in vivo* information on the random Brownian motion of free water and is quantified by the calculation of apparent diffusion coefficients (ADCs). The contrast in the resulting images results from differing signal loss from hydrogen proton movement[1,2]. DWI has extensively been used in tumor grading[3,4], early detection or differential diagnosis of benign and malignant tumors[5–8], distinguishing viable and necrotic tissues[9–12], assessment of organ function[13], prediction of pathologic outcomes[14,15], and evaluation of tumor response to therapies[16–19].

Unfortunately, DWI is sensitive to inhomogeneity of the magnetic field and vulnerable to artefacts with long echo train time[20], especially for when used on small experimental animals. In previous studies the uniformity of the magnetic field was generally improved either by reducing diameter of the coil or by increasing the magnetic field intensity; however, most high quality anatomical images were more concentrated in solid organs, and few in hollow organs[21,22]. Moreover, no relatively detailed studies exist comparing methods for improving DWI. In addition, the poor inhomogeneity of the magnetic field at the air-tissue interface produces severe susceptibility artefacts[1,20,23], with higher magnetic field intensity resulting in more severe artefacts. Some researchers have attempted immersing experimental animals in liquid to isolate such air-tissue interface effects, and achieved interesting results[24]. However, if the liquid is flowing, the imaging position of experimental animals and coil size are significantly restricted, limiting further improvement in DWI quality. It is also difficult to achieve constant temperature for liquids, which proves a great challenge for the longitudinal observation and scanning duration of experimental animals.

On the other hand, diffusion-weighted images with different b values reflect the different restricted degree of water molecules movement. This signal loss of water molecules can be obtained quantitatively with two images of different b values[10]. Due to the serious deformation, artefacts and poor co-registration of diffusion-weighted images with different b values, the accuracy of the ADC value is inevitably affected. Therefore the extension of some research results is limited due to the poor measurement repeatability of ADC values[25].

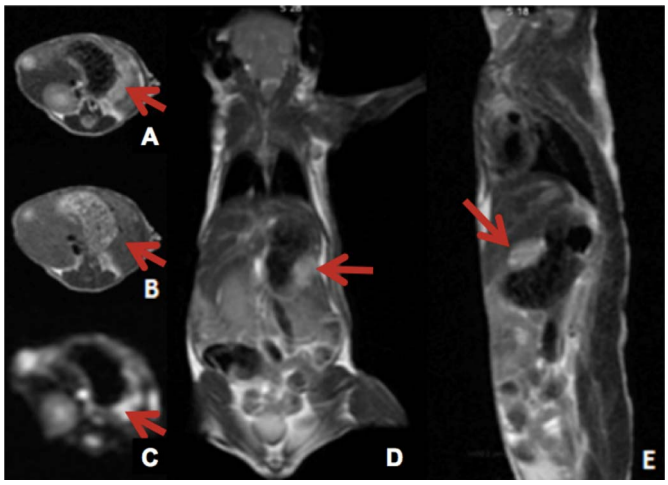

Figure 1 | MR images of gastric cancer for orthotopic mouse model. (A) T2 axial image of orthotopic gastric cancer (red arrows), (B–C) T1 axial image and DW images (with alginate mould) of the same slice. (D–E) T2 coronal and sagittal image of the orthotopic tumour.

To solve the above problems, our research chose the alginate-water mixture together with ultrasonic coupling medium for shaping and isolating the mouse from surrounding air for improved DW imaging. And by comparing the quality of diffusion-weighted images and ADC values of different organs between the alginate and the control group, the improved diffusion-weighted images for the quantitative research of ADC values of experiment animals were obtained. We found the mouse model of orthotopic gastric cancer to be useful in demonstrating the efficacy of this imaging modification in identifying and clarifying internal disease relevant to human conditions.

Results

Orthotopic implantation. Two nude mice died before the first MR scan. Tumours were detected in the stomach of all fourteen remaining nude mice by MRI (red arrows, Figure 1), especially in DW imaging. The subsequent six MR scans were well-tolerated by all fourteen mice.

DW imaging with and without the mould. The container and mouse with and without the alginate mould are shown in Figure 2. The DW images obtained from the two groups with and without the alginate mould, scanned from 7 to 42 days after orthotopic implantation, are shown in Figure 3. The scoring system utilized is shown in Table 1. The artefact and distortion of DW images were greatly reduced in the alginate mould group, and the two observing radiologists were in agreement concerning image rating (kappa coefficient = 0.84, $p < 0.01$). In the group imaged with the alginate mould, the average score of the DW images in outline, distortion, and artefacts were 2.71, 2.92 and 2.90, while the average score of the control group were 1.53, 1.51 and 2.16, respectively (Table 2). From these results, we determined that distortion of DW images was best inhibited in the alginate mould group. As the total score of the mould and control groups were 8.53 and 5.20, respectively, the imaging quality of the alginate mould group was significantly improved ($p < 0.001$). The total score distributions in the two groups are shown in Figure 4. For both DWI and T2 images, the signal-to-noise ratios (SNR) of the tumour between the two groups were not significantly different ($p = 0.934$ for DWI and $p = 0.948$ for T2 sequence) (Supplemental Table 1).

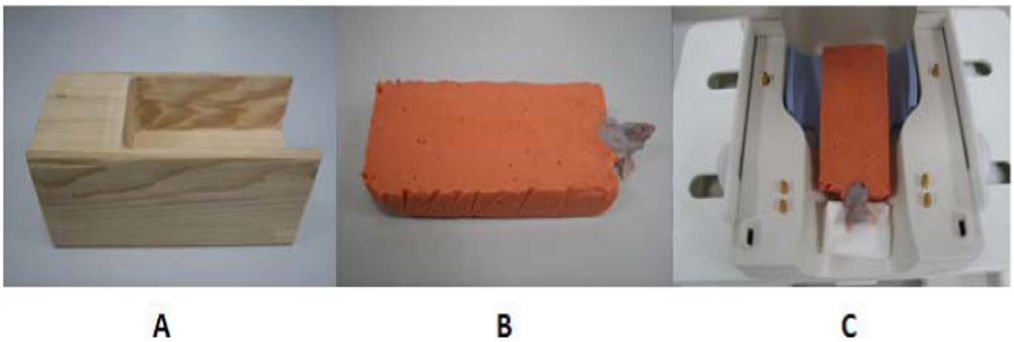

Figure 2 | Alginate mould preparation. (A) The mould for pouring alginate powder mixed with warm water to form the imaging mould. (B) The solid alginate-mouse chamber 30–60 s after liquid alginate was poured around the mouse. (C) The alginate-mouse chamber shaped for the wrist coil.

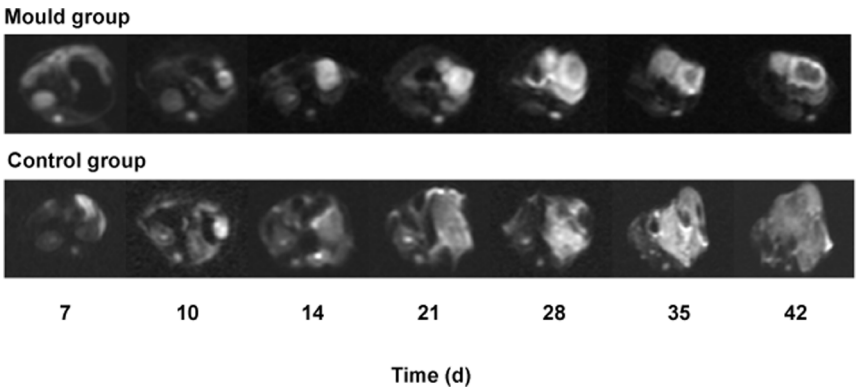

Figure 3 | Diffusion weighted images of mouse with gastric cancer from 7 to 42 days after orthotopic implantation.

Table 1 | Diffusion weighted imaging quality scoring system

Category	Index	Grading Standard
Outline	3	smooth, clear and continuous
	2	uneven but continuous
	1	interrupted
Morphology	3	Same as T2
	2	mild distortion: elongated less than half the major tumour axis
	1	severe distortion: elongated more than half the major tumour axis
Artefacts	3	interior
	2	interior and either dorsal or ventral
	1	interior, dorsal, and ventral

ADC stability using the alginate mould. The ADC values and coefficient of variation (CV) in the normal liver of each mouse in both the mould and control groups are provided in Table 3. The mould group exhibited much less variation (CV = 0.07) compared with those obtained without use of the mould (CV = 0.27), $p < 0.001$ (Figure 5).

The ADC of orthotopic gastric cancer in vivo. From the above results, we determined that the mould group provided not only clearer and less distorted images, but also measurements with high repeatability. Therefore, we used data obtained from the alginate mould group to assess ADC changes of the orthotopic tumour. We used alginate moulding in the serial monitoring of tumour growth by DWI of orthotopic nude gastric cancer. All 7 orthotopic transplanted nude mice survived subsequent seven serial MR scans. The maximum tumour areas increased rapidly during the first 28 days after which growth decelerated (Figure 6A). However, ADC values gradually decreased within 10–30 days after transplantation, and these values increased slightly with tumour growth (Figure 6B). No significant correlation was detected between ADC and the maximum area of the orthotopic tumour ($r = 0.06$, $P = 0.733$).

Discussion

Restricted by sequence design, DWI images exhibit obvious deformation and artefacts, especially for small experimental animals. In addition, the accuracy of ADC value measurement can also be affected. Our study attempted to improve the disadvantages of DWI using homemade scanning mould material. Commonly used dental alginate with superior water solubility, fast solidification, high safety, and appropriate flexibility was applied to pre-positioned experimental animals[26,27]. Our goal in using such an alginate mould was to suppress DWI image deformation and artefacts, estimate DWI image quality and the impact of ADC values, and subsequently choose improved DWI images for ADC value quantitative research.

In the subjective evaluation of DWI imaging in our study, alginate embedding reduced the density difference at the mouse-medium interface compared to a mouse-air interface. The uniformity of the magnetic field around the mice was indirectly improved, and image distortion was suppressed. The DWI deformation occurred primarily due to poor uniformity of the surrounding magnetic field[20,28]. Image distortion was inhibited to some extent by increasing the magnetic field intensity or reducing the inside diameter of the coil, especially for deep solid organs[5,29,30]. However, such methods had no inhibitory effects on artefacts caused by subject conditions which usually occurred between regions of significant differences in magnetic susceptibility (animal - air interface), of the chemical shift region (water - lipid interface) and physical movement region[31,32]; therefore, DWI image artefacts of superficial parts of the body were still evident. The susceptibility artifacts were somewhat reduced when mice were scanned in water in a previous study[24], but the particular vessel used for placing mice in water required the animals to be scanned with a coil with large inside diameter, limiting further enhancement in image quality.

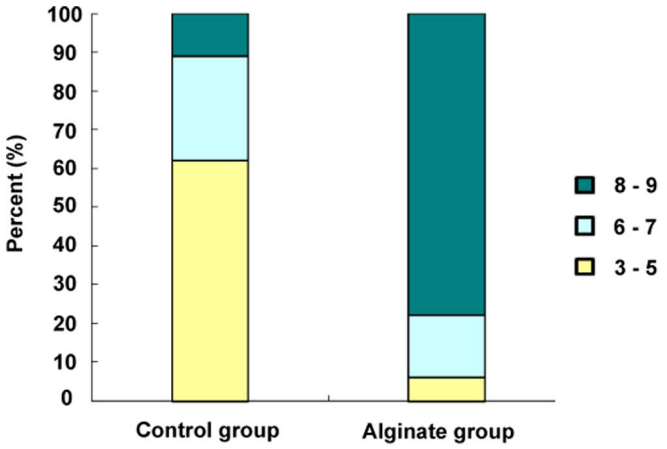

Figure 4 | Stacked percentage bar plot for the total image quality scores for the control and alginate mould groups. Score 8–9 represented high-quality images; Score 6–7 represented moderate-quality images; Score 3–5 represented poor-quality images.

Our study took advantage of the fluidic character of the alginate/water combination to effectively reduce the tissue-air interface, which minimized the difference in magnetic susceptibility between adjacent objects and lessened the surrounding artefacts. Secondly, the alginate mould could be easily shaped to fit different scanning coils, improving the flexibility of its use. In addition, the alginate mould was inexpensive, easily acquired and made. It is also more convenient to use for maintaining animal body temperature during imaging than immersing the animal in water. The alginate mould could enhance the tolerance of the mice to the experimental conditions and increase the feasibility of extended observation durations.

Our imaging results were similar to previous clinical DWI research in the objective evaluation of DWI image quality. If motion artefacts are suppressed, higher intensities are revealed in the ROI and with higher signal-to-noise ratio (SNR), and we found that the alginate mould suppressed deformation, magnetic susceptibility artefacts and improved the SNR of images[32,33]. Secondly, coil load is another factor that could affect the SNR of an image. By using the alginate mould to contain the animal, the volume of the imaged

Table 2 | Scoring for DW images

	Alginate (49 images)			Control (49 images)			
Score	Outline	Distortion	Artifact	Outline	Distortion	Artifact	P value
3	38	46	44	5	2	14	
2	8	2	5	16	21	29	
1	3	1	0	28	26	6	
Average	2.71 ± 0.58	2.92 ± 0.34	2.9 ± 0.31	1.53 ± 0.68	1.51 ± 0.58	2.16 ± 0.62	
Total		8.53 ± 1.12			5.2 ± 1.73		<0.001

Table 3 | Normal liver ADC value ($\times 10^{-3}$ mm^2/sec)

	Alginate			Control			P value
Mouse	Mean	Std	CV	Mean	Std	CV	
1	1.21	0.06	0.05	1.08	0.41	0.38	
2	0.79	0.14	0.18	1.25	0.44	0.35	
3	0.9	0.08	0.08	0.88	0.22	0.25	
4	1.11	0.09	0.08	0.87	0.21	0.24	
5	1.08	0.05	0.05	0.84	0.24	0.29	
6	0.99	0.04	0.04	0.9	0.17	0.19	
7	1.11	0.02	0.02	0.95	0.18	0.19	
X			0.07			0.27	$P < 0.001$

Std: Standard deviation, CV: coefficient of variation.

object could approach the optimal value of the coil, which would enhance capture of signal changes and improve signal intensity. In conclusion, our study shows that distortion and artefacts of DWI were suppressed and the repeatability of ADC values was improved by use of the described alginate mould in a mouse model of orthotopic gastric cancer.

Methods

Cell line and orthotopic stomach tumour implantation. All procedures were performed according to the protocol approved by our institutional review board. A human gastric cancer cell line, BGC-823, was maintained in RPMI 1640 media (Beijing Solarbio Science & Technology Co., Ltd, Beijing, China) supplemented with 10% fetal bovine serum (FBS, Gibco, New York, USA) at 37 ± 2°C, pH 7.2, in a humidified atmosphere of 95% air and 5% CO_2. Cells were passaged and expanded by trypsinization followed by replating every 2–3 days. The culture media was changed every 2 days. For mouse inoculation, cells in log-phase growth were harvested by trypsinization, and medium containing 10% FBS was added. Following centrifugation for 5 min at 1000 rpm, cells were resuspended in phosphate-buffered saline (PBS) and kept at 37 ± 2°C until inoculation.

Anesthetized female athymic 7 week old BALB/c nude mice, maintained under SPF (Specified Pathogen Free) conditions in our hospital's animal facilities, received 5.0×10^6 BGC-823 cells suspended in a volume of 0.2 ml sterile DPBS by subcutaneous injection below the dorsal flank. The mice were observed for the following 3 weeks, after which tumour incidence was determined. Mice were then sacrificed and tumours were removed. The tumour parenchyma was cut into small pieces less than 1 mm^3.

Under anaesthesia of 0.5% amobarbital in 0.1 ml, a small median abdominal incision was made for each of sixteen mice, and then purse-string sutures were performed on the anterior wall of stomach. The sixteen mice were randomly divided into two groups, an alginate group and control group, in this study. The surgeon made a serosal incision within the purse of the anterior wall, and a small piece of tumour was implanted under the subserosal layer. The serosa and purse were both sutured to

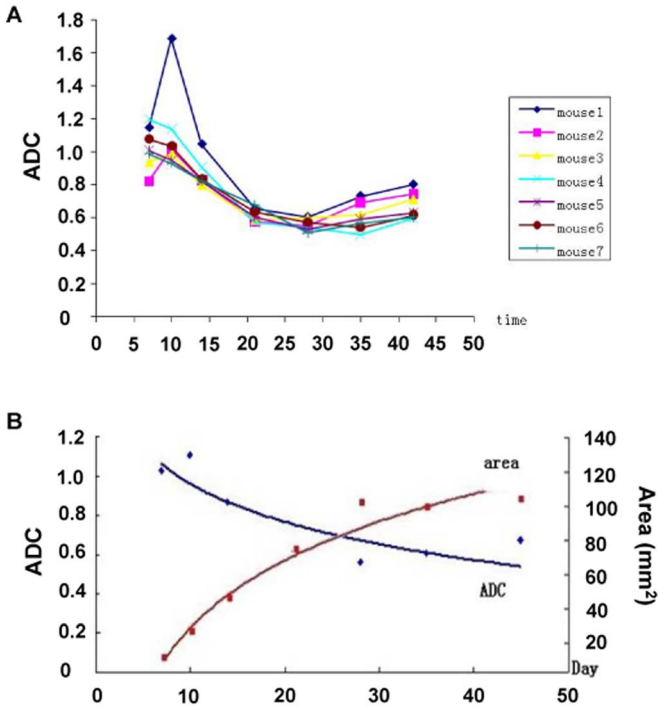

Figure 6 | Longitudinal ADC value and the maximum orthotopic tumour area. (A) Longitudinal ADC value of gastric cancer for each mouse. (B) The average ADC value and average maximum area of the orthopic tumours for all seven mice in each group.

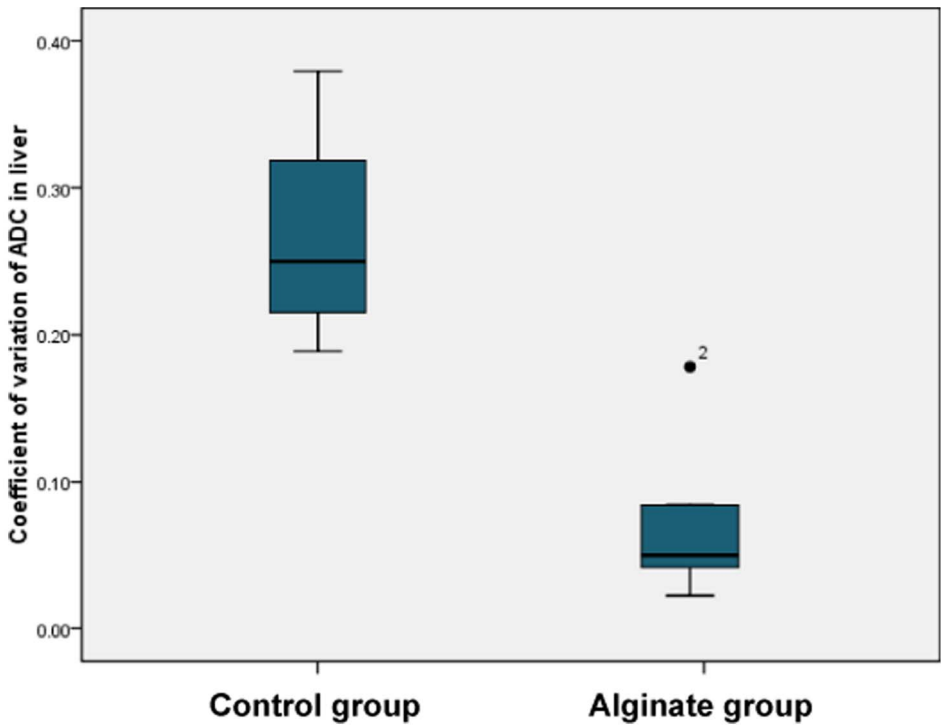

Figure 5 | Box plot for the coefficient of variation of ADC in normal liver.

Table 4 | MRI scanning parameters

Sequence	T1 WI	T2 WI	DWI
TR/TE	400/12	3381/58	2000/minimum
FOV (mm)	60 × 45 (axial)	60 × 30 (axial), 60 × 60 (coronal and sagittal)	80 × 60 (axial)
Matrix	192 × 192	256 × 192	64 × 64
Slice Thickness (mm)	2	2	2
Slice Spacing (mm)	0.2	0.2	0.2
Matrix (mm)	0.3 × 0.2 × 0.2	0.2 × 0.2 × 0.2, 0.2 × 0.3 × 0.2	1.3 × 1.3 × 0.2
Excitation number	4	8	8
Bandwidth (kHz)	22.7	15.6	166.7
Scan Time	3′07″	6′06″ (axial), 4′54″ (coronal and sagittal)	2′16″
b (s/mm^2)			0.1
ET	13	16	-

TR: repetition time, TE: echo delay time, FOV: field of view, ET: echo time.

prevent the tumour from entering the peritoneal cavity. The stomach was then returned to the peritoneal cavity, and the abdominal wall was closed with absorbable suture.

MR imaging. *Alginate-mouse chamber and nude preparation.* As a prerequisite, we developed a mouse-imaging chamber adapted to our wrist joint coil, enabling the head of the mouse to remain outside the chamber for breathing. The alginate (Zhermack, Badia Polesine, Italy) used in our study is a common type often used by dentists for dental impressions. It is commercially available as a ready-to-use powder and solidifies within 2–3 min when mixed with water to a rubbery consistency. We used approximately 150% of the amount of warm water (40–42°C) to reduce viscosity of the mould for improved flow ability and an increased time span until solidification. We then positioned the mouse into the chamber as follows:

For the alginate group, the nude mice were anesthetized by 0.5% amobarbital in 0.1 ml and then overlaid with coupling medium commonly used in ultrasonography in our hospital. We positioned the anesthetized mouse in the chamber with the head outside through the air vent, and then filled the chamber with alginate/water mixture. Finally, the chamber was immobilized in the wrist coil. Control group mice were prepared for MRI scanning with the same procedure as the alginate group, but without the use of coupling medium and alginate filling.

Imaging procedures. To avoid incisional infection of the stomach, the first MR imaging was performed on the seventh day after orthotopic implantation. The 14 total nude mice underwent MR imaging at 7, 10, 14, 21, 28, 35 and 42 days after orthotopic implantation. MRI scanning was performed on a clinical 3T scanner (Discovery MR750 3.0T, GE Healthcare, Milwaukee, WI, USA) using an 8-channel HD Wrist Array coil for the mouse abdomen. A total of 7 scans were performed at each time point for each animal for a total of 49 obtained images for each of the control and alginate groups. Prior to DW imaging, all mice underwent examination with routine gastric MR protocols to localize the tumours and provide morphologic details. The MR sequencing parameters are detailed in Table 4.

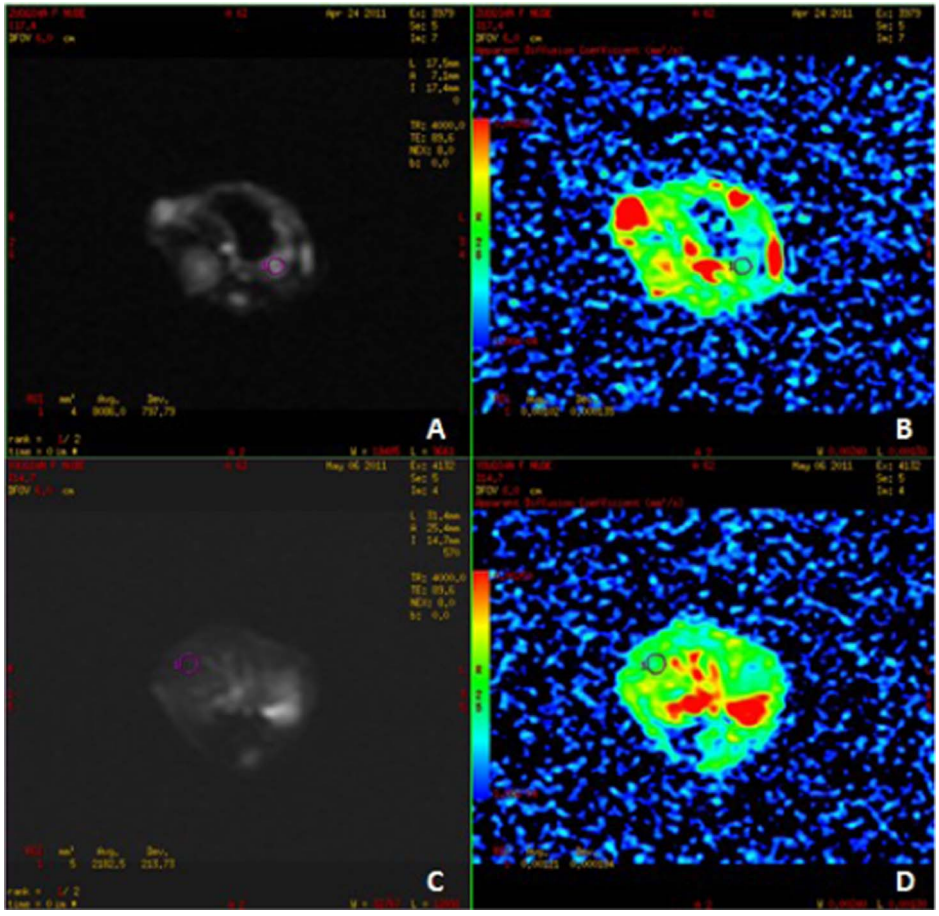

Figure 7 | ROI in the orthotpic gastric cancer and normal liver. (A–B) ROI in the orthotopic tumour and its ADC value. (C–D) ROI in the normal liver and its ADC value.

Image analysis and scoring system of DWI imaging quality. All DW images were analysed independently by two experienced radiologists (X.Y.Z. and L.T., with 6 and 10 years' experience in MR, respectively), working on a workstation (AW4.4; GE Medical Systems, Waukesha, WI, USA), and using a scoring system based upon the following. The total score equalled the sum score of the three indexes shown in Table 1. Score 8–9 represented high-quality images; Score 6–7 represented moderate-quality images; Score 3–5 represented poor-quality images.

ROI designation and quantification. The regions of interest (ROI) were drawn by the consensus between two radiologists.

Liver: ROIs were manually drawn cross images of the liver with an area of approximately 5 mm^3 excluding the vessels and bile ducts. The ADC of each ROI was recorded and an average ADC was obtained (Figure 7).

Tumour: After identification of an orthotopic gastric tumour, ROIs were manually drawn with the same areas of the tumour in T2 images. The ADC of each ROI was recorded and an average ADC was obtained for each lesion. The longest diameter and the vertical diameter of the tumour were also recorded. We used the product of these two diameters as the maximum area of the tumour (Figure 7).

Statistical analysis. All statistical analysis was conducted with SPSS statistical software (Version 15.0. Chicago IL, USA). Continuous data were expressed as median and range or mean $\pm$ SD. Coefficient of variation (CV) was used to assess the degree of variation. A two-tailed student's t-test was used to compare values between the alginate and control groups. One-way analysis of variance (ANOVA) was utilized to detect differences in CV of hepatic ADC value between animals across within the alginate and non-alginate groups. A Mann–Whitney U test was used to compare the sum score for image quality between the alginate and control groups. A bar chart was drawn to display the distribution of the sum score for image quality. The changing trends of ADC values and the maximum area of orthotopic tumours were illustrated using a scatter diagram. The Kappa coefficient was calculated to measure the inter-rater agreement (0–0.20 as slight, 0.21–0.40 as fair, 0.41–0.60 as moderate, 0.61–0.80 as substantial, and 0.81–1 as perfect agreement). The correlation between ADC value and the maximum area of tumour was assessed with Pearson's correlation coefficient. A p value < 0.05 indicated statistical significance.

1. Chen, F. *et al.* Diffusion weighted imaging in small rodents using clinical MRI scanners. *Methods* **43**, 12–20, doi:10.1016/j.ymeth.2007.03.007 (2007).
2. Rau, P. R. *et al.* Apparent diffusion coefficient in the aging mouse brain: a magnetic resonance imaging study. *Life Sci.* **78**, 1175–1180, doi:10.1016/j.lfs.2005.06.032 (2006).
3. Price, S. J. *et al.* Predicting patterns of glioma recurrence using diffusion tensor imaging. *Eur. Radiol.* **17**, 1675–1684, doi:10.1007/s00330-006-0561-2 (2007).
4. Hayashida, Y. *et al.* Diffusion-weighted imaging of metastatic brain tumors: comparison with histologic type and tumor cellularity. *AJNR. Am. J. Neuroradiol.* **27**, 1419–1425 (2006).
5. Song, S. K. *et al.* Improved magnetic resonance imaging detection of prostate cancer in a transgenic mouse model. *Cancer Res.* **62**, 1555–1558 (2002).
6. Eida, S., Sumi, M., Sakihama, N., Takahashi, H. & Nakamura, T. Apparent diffusion coefficient mapping of salivary gland tumors: prediction of the benignancy and malignancy. *AJNR. Am. J. Neuroradiol.* **28**, 116–121 (2007).
7. Smith, J. S. *et al.* Limitations of diffusion-weighted imaging in distinguishing between a brain tumor and a central nervous system histoplasmoma. *J. Neuro-oncol.* **79**, 217–218, doi:10.1007/s11060-005-9007-y (2006).
8. Rumboldt, Z., Camacho, D. L., Lake, D., Welsh, C. T. & Castillo, M. Apparent diffusion coefficients for differentiation of cerebellar tumors in children. *AJNR. Am. J. Neuroradiol.* **27**, 1362–1369 (2006).
9. Lyng, H., Haraldseth, O. & Rofstad, E. K. Measurement of cell density and necrotic fraction in human melanoma xenografts by diffusion weighted magnetic resonance imaging. *Magn. Reson. Med.* **43**, 828–836 (2000).
10. Herneth, A. M., Guccione, S. & Bednarski, M. Apparent diffusion coefficient: a quantitative parameter for in vivo tumor characterization. *Eur. J. Radiol.* **45**, 208–213 (2003).
11. Reddy, J. S. *et al.* The role of diffusion-weighted imaging in the differential diagnosis of intracranial cystic mass lesions: a report of 147 lesions. *Surg. Neurol.* **66**, 246–250; discussion 250–241, doi:10.1016/j.surneu.2006.03.032 (2006).
12. Koc, O., Paksoy, Y., Erayman, I., Kivrak, A. S. & Arbag, H. Role of diffusion weighted MR in the discrimination diagnosis of the cystic and/or necrotic head and neck lesions. *Eur. J. Radiol.* **62**, 205–213, doi:10.1016/j.ejrad.2006.11.030 (2007).
13. Thoeny, H. C. & De Keyzer, F. Extracranial applications of diffusion-weighted magnetic resonance imaging. *Eur. Radiol.* **17**, 1385–1393, doi:10.1007/s00330-006-0547-0 (2007).
14. Hand, P. J. *et al.* MR diffusion-weighted imaging and outcome prediction after ischemic stroke. *Neurology* **66**, 1159–1163, doi:10.1212/01.wnl.0000202524.43850.81 (2006).
15. Khan, R. B. *et al.* Use of diffusion weighted magnetic resonance imaging in predicting early postoperative outcome of new neurological deficits after brain tumor resection. *Neurosurgery* **59**, 60–66; discussion 60–66, doi:10.1227/01.NEU.0000219218.43128.FC (2006).
16. Cui, Y., Zhang, X. P., Sun, Y. S., Tang, L. & Shen, L. Apparent diffusion coefficient: potential imaging biomarker for prediction and early detection of response to chemotherapy in hepatic metastases. *Radiology* **248**, 894–900, doi:10.1148/radiol.2483071407 (2008).
17. Reichardt, W., Juettner, E., Uhl, M., Elverfeldt, D. V. & Kontny, U. Diffusion-weighted imaging as predictor of therapy response in an animal model of Ewing sarcoma. *Invest. Radiol.* **44**, 298–303, doi:10.1097/RLI.0b013e31819dcc84 (2009).
18. Sun, Y. S. *et al.* Locally advanced rectal carcinoma treated with preoperative chemotherapy and radiation therapy: preliminary analysis of diffusion-weighted MR imaging for early detection of tumor histopathologic downstaging. *Radiology* **254**, 170–178, doi:10.1148/radiol.2541082230 (2010).
19. Tang, L. *et al.* Gastrointestinal stromal tumors treated with imatinib mesylate: apparent diffusion coefficient in the evaluation of therapy response in patients. *Radiology* **258**, 729–738, doi:10.1148/radiol.10100402 (2011).
20. Le Bihan, D., Poupon, C., Amadon, A. & Lethimonnier, F. Artifacts and pitfalls in diffusion MRI. *J. Magn. Reson. Imaging: JMRI* **24**, 478–488, doi:10.1002/jmri.20683 (2006).
21. Berr, S. S., Roche, J. K., El-Rifai, W., Smith, M. F., Jr. & Powell, S. M. Magnetic resonance imaging of gastric cancer in Tff1 knock-out mice. *Magn. Reson. Med.* **49**, 1033–1036, doi:10.1002/mrm.10458 (2003).
22. Zieker, D. *et al.* Phosphoglycerate kinase 1 promoting tumor progression and metastasis in gastric cancer - detected in a tumor mouse model using positron emission tomography/magnetic resonance imaging. *Cell. Physiol. Biochem.* **26**, 147–154, doi:10.1159/000320545 (2010).
23. van den Bos, I. C., Hussain, S. M., Krestin, G. P. & Wielopolski, P. A. Liver imaging at 3.0 T: diffusion-induced black-blood echo-planar imaging with large anatomic volumetric coverage as an alternative for specific absorption rate-intensive echo-train spin-echo sequences: feasibility study. *Radiology* **248**, 264–271, doi:10.1148/radiol.2481070034 (2008).
24. Zhang, X. Y., Sun, Y. S., Tang, L., Xue, W. C. & Zhang, X. P. Correlation of diffusion-weighted imaging data with apoptotic and proliferation indexes in CT26 colorectal tumor homografts in balb/c mouse. *J. Magn. Reson. Imaging: JMRI* **33**, 1171–1176, doi:10.1002/jmri.22558 (2011).
25. Jovicich, J. *et al.* Reliability in multi-site structural MRI studies: effects of gradient non-linearity correction on phantom and human data. *NeuroImage* **30**, 436–443, doi:10.1016/j.neuroimage.2005.09.046 (2006).
26. Rommel, D. *et al.* Alginate moulding: an empirical method for magnetic resonance imaging/positron emission tomography co-registration in a tumor rat model. *Nucl. Med. Biol.* **35**, 571–577, doi:10.1016/j.nucmedbio.2008.04.002 (2008).
27. Strobel, K., Bergmann, R., Meister, S., van den Hoff, J. & Pietzsch, J. Improved multimodality imaging using alginate molding in xenograft tumor models. *J. Magn. Reson. Imaging: JMRI* **31**, 747–752, doi:10.1002/jmri.22090 (2010).
28. Farzaneh, F., Riederer, S. J. & Pelc, N. J. Analysis of T2 limitations and off-resonance effects on spatial resolution and artifacts in echo-planar imaging. *Magn. Reson. Med.* **14**, 123–139 (1990).
29. Callot, V., Duhamel, G., Cozzone, P. J. & Kober, F. Short-scan-time multi-slice diffusion MRI of the mouse cervical spinal cord using echo planar imaging. *NMR Biomed.* **21**, 868–877, doi:10.1002/nbm.1274 (2008).
30. Kim, H. *et al.* Early therapy evaluation of combined anti-death receptor 5 antibody and gemcitabine in orthotopic pancreatic tumor xenografts by diffusion-weighted magnetic resonance imaging. *Cancer Res.* **68**, 8369–8376, doi:10.1158/0008-5472.CAN-08-1771 (2008).
31. Kuhl, C. K., Traber, F. & Schild, H. H. Whole-body high-field-strength (3.0-T) MR Imaging in Clinical Practice. Part I. Technical considerations and clinical applications. *Radiology* **246**, 675–696, doi:10.1148/radiol.2463060881 (2008).
32. Jansen, J. F., Backes, W. H., Nicolay, K. & Kooi, M. E. 1H MR spectroscopy of the brain: absolute quantification of metabolites. *Radiology* **240**, 318–332, doi:10.1148/radiol.2402050314 (2006).
33. Ozaki, M. *et al.* Motion artifact reduction of diffusion-weighted MRI of the liver: use of velocity-compensated diffusion gradients combined with tetrahedral gradients. *J. Magn. Reson. Imaging: JMRI* **37**, 172–178, doi:10.1002/jmri.23796 (2013).

Acknowledgments

This work was supported by the National Basic Research Program of China (973 Program) (Grant No. 2011CB707705) and National Natural Science Foundation of China (Grant No. 81371715, 81201215), Capital Foundation of Medical Developments (Grant No. 2011-2015-02) and Beijing Health System High Level Health Technical Personnel Training Plan (No.2013-3-083). We would like to thank Clarity Manuscript Consultants LLC for technical assistance in editing this manuscript.

Author contributions

J.S. designed and performed experiments, and wrote the manuscript, X.P.Z. advised and instructed experimental design and procedures, X.T.L. performed statistical analysis and experiments, and L.T., Y.C., X.Y.Z. and Y.S.S. all performed experiments in the study.

Additional information

Supplementary information accompanies this paper at http://www.nature.com/scientificreports

Competing financial interests: The authors declare no competing financial interests.

How to cite this article: Sun, J. *et al*. Applicable apparent diffusion coefficient of an orthotopic mouse model of gastric cancer by improved clinical MRI diffusion weighted imaging. *Sci. Rep.* **4**, 6072; DOI:10.1038/srep06072 (2014).